

Chandra Observations of Six QSOs at $z \approx 3$ ¹

Takamitsu Miyaji

Physics Department, Carnegie Mellon University, 5000 Forbes Ave., Pittsburgh, PA 15213
miyaji@cmu.edu

Günther Hasinger, Ingo Lehmann¹

Max-Planck Institut für extraterrestrische Physik, Postf. 1312, 85741 Garching, Germany

Donald P. Schneider

Department of Astronomy and Astrophysics, 525 Davey Laboratory, Pennsylvania State University,
University Park, PA 16802

ABSTRACT

We report the results of our Chandra observations of six QSOs at $z \approx 3$ from the Palomar Transit Grism Survey. Our primary goal is to investigate the possible systematic change of α_{ox} between $z > 4$ and $z \approx 3$, between which a rapid rise of luminous QSO number density with cosmic time is observed. The summed spectrum showed a power-law spectrum with photon index of $\Gamma = 1.9$, which is similar to other unabsorbed AGNs. Combining our $z \approx 3$ QSOs with X-ray observations of QSOs at $z > 4$ from literature/archive, we find a correlation of α_{ox} with optical luminosity. This is consistent with the fact that the luminosity function slope of the luminous end of the X-ray selected QSOs is steeper than that of optically-selected QSOs. We discuss an upper limit to the redshift dependence of α_{ox} using a Monte-Carlo simulation. Within the current statistical errors including the derived limits on the redshift dependence of α_{ox} , we found that the behaviors of the X-ray and optically-selected QSO number densities are consistent with each other.

Subject headings: galaxies: active | galaxies: high-redshift | galaxies: luminosity function | (galaxies:) quasars: general | X-rays: galaxies

1. Introduction

Large-scale optical surveys show that the luminous QSO number density peaks at $1.7 < z < 2.7$, before which (in cosmic time) the QSO number density grows rapidly and after which the density steadily decays until the present epoch (e.g. Boyle et al. 1988; Warren, Hewett, & Osmer 1994; Schmidt, Schneider, & Gunn 1995). The first indication of a density decline (with redshift) at

$z \approx 3$ was reported in the pioneering work of Osmer (1982). The Palomar Transit Grism Survey (PTGS) (Schneider, Schmidt, & Gunn 1994) was designed to investigate this possible "redshift cutoff", and produced a sample of 90 $z > 2.7$ QSOs; an analysis of the PTGS Schmidt, Schneider, & Gunn (1995) (hereafter SSG95) revealed a very rapid growth, by a factor of ≈ 3.5 , of the number density of luminous QSOs from $z \approx 4.5$ to 2.7 . This result was verified by Fan et al. (2001) using a sample of $3.6 < z < 5.0$ quasars found in the Sloan Digital Sky Survey (SDSS; York et al. 2000). This redshift cutoff has also been found in the number densities of radio-*at*-spectrum QSOs

¹Present Address: LP S-Berlin, Kopernikerstr. 325, 12555, Berlin, Germany

¹Based on observations using the Chandra X-ray Observatory.

(Shaver et al. 1996; Wall et al. 2005).

In the X-ray regime, however, the size of a sample based on the combination of various ROSAT surveys, Miyaji, Hasinger, & Schmidt (2000) (hereafter, SXLF1) was not sufficient to accurately probe this "growth" phase of the number density of X-ray-selected luminous ($\log L_x > 44.5$) QSOs. While this study appears to show a flat number density in $z > 2.7$, the uncertainties produced by the small number of quasars limited the robustness of the conclusions. More recent studies including the results from Chandra and XMM-Newton surveys (Cowie et al. 2003; Fiore et al. 2003; Ueda et al. 2003; Barger et al. 2005) showed that the number density curve is luminosity-dependent and a trend that as luminosity goes lower, the density peak shifts to lower redshifts (as some authors call an anti-hierarchical AGN evolution and others call a down-sizing of the AGN activity). However, these studies did not sample well the high-redshift, high-luminosity regime, in which optically selected QSOs show a decline at $z > 3$.

In a recent study based on an updated soft X-ray sample including Chandra and XMM-Newton surveys, Hasinger, Miyaji & Schmidt (2005) (hereafter SXLF3) also measured the number densities in various luminosity bins with a better accuracy over a large range in the redshift-luminosity space. The study revealed this early "growth" of AGN number density (or decline with increasing z) at $z \lesssim 3$ for AGN/QSO luminosities at ($\log L_x \sim 44-45$). The results from "Champs" survey, which was designed to optimally trace the high-redshift, high-luminosity ($\log L_x > 44.5$) regime with improved statistics, found that the density curves X-ray selected QSOs ($\log L_x > 44.5$) declines with increasing redshift at $z > 3$. This decline is, however, shallower than that seen in optically-selected QSOs.

The dependence of the optical to X-ray flux ratio (customarily expressed by the quantity α_{ox} , the effective spectral index between the rest-frame 2500 Å and 2 keV)² on redshift and luminosity has been a key issue in X-ray observations of high-redshift QSOs and has important implications for possible differences in the AGN evolution traced by X-ray and optical samples. Some authors (e.g. Vignali, Brandt, & Schneider 2003b; Strateva et

al. 2005) found that α_{ox} strongly depends on luminosity, with $L_x / L_{opt}^{0.75}$, and no evidence for any evolution of the X-ray properties with redshift. Bechtold et al. (2003) found that variations in α_{ox} depends primarily on redshift. The dependence may be sensitive to the selection effects, including but not limited to whether the sample is optically-selected or X-ray selected. Yuan et al. (1998b) pointed out that such an apparent non-linearity of the luminosity correlation in two bands can arise from the difference in the luminosity variations in the two bands.

In order to investigate the redshift dependence of the optical-to-X-ray luminosity ratios and its impact on the density curves of luminous QSOs in X-ray and optically selected samples at $z \lesssim 3$, we have obtained Chandra observations of six PTGS QSOs with redshifts between 2.91 and 2.96. This is the era of maximum number density of luminous QSOs. There was practically no systematic observations in X-rays in this redshift regime before. Thus our observations also serve to fill this observation gap. Throughout this paper we adopt (H_0 [km s⁻¹ pc⁻¹]; Ω_m ; Ω_Λ) = (70; 0.3; 0.7) and $h_{70} = 1$ unless otherwise noted.

2. Observations and Analysis

2.1. The Sample and Observation

The original motivation of the program was to compare the mean α_{ox} values of $z \lesssim 3$ and $z \lesssim 4$ QSOs. In Chandra Cycle 4, six $z \lesssim 3$ QSOs from the PTGS (out of 15 QSOs proposed) have been observed. None of these QSOs are broad absorption line (BAL) QSOs. Table 1 shows the observed targets, log of observations, optical AB magnitudes at the object's rest frame of 1450 Å. The core radio loudness $R_L = \log_{10} f_{20cm} / f_{4000Å}$ is also shown, where those with $R_L \leq 1$ and > 1 are divided into radio-quiet QSOs (RRQ) and radio-loud QSOs (RLQ) respectively (Wilkes 2000 and references therein). The fluxes are in the object's rest frame, calculated assuming radio and optical spectral indices of $\alpha_r = 0.8$ and $\alpha_o = 0.79$ respectively. The radio data are from the NVSS (PC 0041+0024 Condon et al. 1998) or FIRST (all others Becker, White, & Helfand 1995) surveys. Only one QSO (PC 1035+4747) was detected in the radio band and for others, 3 upper limits of

²We use f / ν^{α} , where α is any subscript to ν .

R_L are shown. The only radio-detected QSO, PC 1035+ 4747, has $R_L = 2.3$; this object falls well into the RLQ regime. Two of the R_L upper limits (1.5 for PC 0041+ 0214 and 1.2 for PC 1000+ 4751) are above the RQQ/RLQ border, but their limits are well below the peak of the R_L distribution of RLQ. Thus we tentatively classify them as RQQs.

All observations have been made with the Advanced CCD Imaging Spectrometer (ACIS; Garnire et al. 2003) and the targets aimed at the default position of ACIS-S with the S3-chip. In all cases except PC 0947+ 5628, X-ray counterparts have been found within $1.5''$ of the cataloged optical center of the target QSOs, consistent with the combined systematic error on the absolute astrometries of $1''-2''$ in both the Chandra data products and the PTGS survey. Although the detected X-ray source closest to PC 0947+ 5628 was $2.8''$ away from the cataloged position of the QSO, 6 other X-ray sources in the same ACIS observation also had optical counterparts at $2.8''$ away with practically the same offset directions. Thus we also identify the X-ray source with PC 0947+ 5628.

2.2. Individual and Stacked Spectra

For all six observations, we have extracted the pulse-height spectra using an extraction radius of $2''$. Spectra, response matrices (rmf) and ancillary response files (arf) were created using the software package CIAO 3.0.2 or later versions, in conjunction with the calibration database CALDB 2.2.6 or later versions. These versions enabled construction of the response files which takes the time-dependent low energy efficiency degradation into account. Due to low number counts of the involved objects, changes due to further updates of the calibration have negligible effects. The spectral analyses were made to the pulse-height channels corresponding to observed photon energies of 0.3–7 keV. Background level is typically 0.05 counts in the extraction radius and is thus negligible. The spectral analysis were made with XSPEC 11.2. In spite of small number of X-ray photons, the negligible background and the use of the XSPEC implementation of the Cash (1979) C -statistics allowed placement of some constraints on the spectral indexes, although there are not sufficient number of photons in any individual spectrum to simultaneously constrain the intrinsic absorption column density. The results of the

spectral fits with a single power-law with a photon index Γ and the Galactic absorption N_{H20}^G [cm²] Dickey & Lockman (1990) at the position of the QSOs are shown in Table 2. We see that the only radio-detected QSO's photon index of $\Gamma = 0.4 \pm 0.1$ is constrained to be harder than the mean QSO spectrum. The rest-frame 2–10 keV luminosities ($\log L_x$; logarithm is base-10) are also shown as well as the source counts in 0.3–7 keV. The rest-frame 2–10 keV corresponds to observed frame 0.5–2.5 keV. The B-band absolute magnitudes (M_B), that have been recalculated using our default cosmology (Sect. 1) and the optical spectral index $\alpha = 0.79$ (following Vignali et al. 2003c; Fan et al. 2001), are also listed here. Using $\alpha = 0.5$ (Schneider et al. 2001) increases M_B by 0.35.

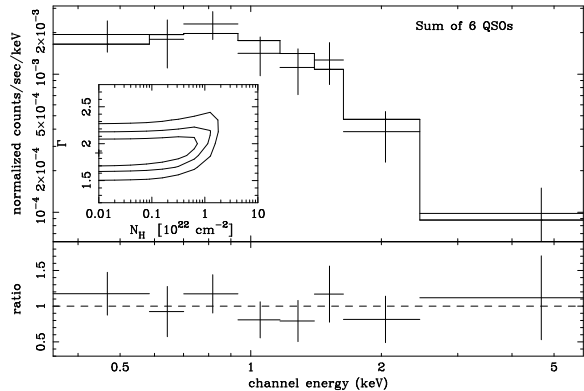


Fig. 1. | The stacked pulse-height spectrum of the 6 QSOs at $z = 3$ with the folded best-fit power-law model and residuals in terms of the data-to-model ratio. The spectrum is rebinned for display, but the actual fit was made to a higher resolution. Confidence contours at levels of $C = 2.3$ and 4.6, 9.2 (corresponding to the 68%, 90% and 99% confidence levels for two interesting parameters respectively) in the N_{H22} plane are also shown.

We also analyzed the summed spectrum from all six QSOs. Because of the small spread of the redshifts of these QSOs, we can analyze the summed spectrum assuming a single redshift. The response matrix for the summed spectrum was constructed by a source-count weighted mean of the matrices. The Galactic column densities $N_{\text{H}20}^{\text{G}}$ of these six QSOs are 0.9, 1.0, 1.0, 1.3, 2.0 and 2.8. The fit was made to a model with the sum of three power-laws, with different Galactic absorptions of $N_{\text{H}20}^{\text{G}} = 1.0; 2.0$ and 2.8 respectively, where the four QSOs with $0.9 < N_{\text{H}20}^{\text{G}} < 1.3$ were represented by a single column density of 1.0. The photon indices of all the three components were set to equal and the ratios of the 3 normalizations were fixed to those of the total source counts of the QSOs with $N_{\text{H}20}^{\text{G}}$ of 0.9-1.3, 2.0 and 2.8 respectively. Also an intrinsic absorption component $N_{\text{H}20}^{\text{Z}}$ is included with $z = 2.93$, which is a source-count weighted mean redshift of the sample. Again, the C-statistics was used for the fit. The summed spectrum is well represented by a single power-law with $\Gamma = 1.9$ and no intrinsic absorption, as shown in the last entry of Table 2. The pulse-height spectrum, folded best-fit power-law model, and fit residuals in terms of data-to-model ratio are shown in Fig. 1, with confidence contours for the intrinsic absorption versus photon index space. Removing the one RLQ (PC 1035+ 4747) from the analysis did not change the fitted parameters and errors to the smallest digits displayed in Table 2. This result is consistent with the mean slopes of RLQs and unabsorbed AGNs measured in the 2-10 keV in the rest frame over a wide range of redshift and luminosity (e.g. Vignali et al. 2003a,c). Note, however, that the stacked spectrum is dominated by a few brightest sources, with 60% of the photons coming from the two brightest objects. The quoted error only includes the statistical error of photon counts. The sampling error is estimated by a bootstrapping method, where the 90% error range was determined by 500 bootstrap runs of a photon-count weighted mean best-fit values. The results were (90% bootstrap errors) $\Gamma = 1.85^{+0.31}_{-0.25}$ (1.97 \pm 0.29 with the RLQ removed).

2.3. The Optical to X-ray Index (α_{ox})

The optical (rest-frame ultraviolet) to X-ray flux ratio of a QSO is customarily expressed in

terms of the effective index α_{ox} between 2 keV and 2500Å in the QSO rest frame. Upon calculating α_{ox} , we assumed $\beta = 2.0$ for all, which is the average QSO spectral index. The result of the spectral analysis of all but one is consistent with the canonical spectral index of $\beta = 1.9-2.0$. The RLQ PC 1035+ 4747 has $\beta = 0.6 \pm 0.8$ and using $\beta = 0.6$ for K-correction gives $\alpha_{\text{ox}} = -2.06$. Other than this one, the main source of errors in α_{ox} is the X-ray flux. Even for the source with the smallest source count (PC 1035+ 4747) the 1 σ error on α_{ox} is 0.05. A decrease of β by 0.2 leads to an increase of α_{ox} by 0.04 at $z = 3$. Using $\beta = 0.5$ instead of 0.79, α_{ox} increases by 0.03.

3. Redshift and M_{B} Dependences of α_{ox}

This program is mainly focused on the systematic difference in α_{ox} between $z < 3$ and $z > 4$. Because α_{ox} values of QSOs show a large scatter and we only sample a small number of QSOs in the redshift-luminosity regimes of our interest, the sampling error is the dominant effect in the error budget of the mean value $\langle \alpha_{\text{ox}} \rangle$ of QSOs, which can be estimated by $\sigma_{\alpha_{\text{ox}}} = \frac{\sigma_{\alpha_{\text{ox}}}}{N_{\text{Q}}}$, where $\sigma_{\alpha_{\text{ox}}}$ is the standard deviation of the α_{ox} distribution of N_{Q} QSOs. Note that the $\sigma_{\alpha_{\text{ox}}} = \frac{\sigma_{\alpha_{\text{ox}}}}{N_{\text{Q}}}$ estimation of the standard deviation of the mean is also valid for small N_{Q} . It is well known that this estimator gives the exact confidence range of Gaussian 1 σ when the parent α_{ox} distribution is a Gaussian and it is widely used in more general cases. The α_{ox} distributions in Yuan et al. (e.g. 1998a); Strateva et al. (e.g. 2005); Vignali, Brandt, & Schneider (e.g. 2003b) are well characterized by a Gaussian, which justifies the use of this estimator in our analysis. For our sample, we obtain $\langle \alpha_{\text{ox}} \rangle = -1.65 \pm 0.05$ (-1.62 ± 0.05 , for the 5 RLQs only). Our results are compared with those of $z < 4$ QSOs in Table 4. Ideally, we would like to compare with $z > 4$ QSOs in the same luminosity range ($-27.0 < M_{\text{B}} < -26.3$)³. Unfortunately all but a few of the $z > 4$ QSOs observed previously with X-rays found in literature (Bechtold et al. 2003; Vignali et al. 2001, 2003a, 2005) are more luminous ($M_{\text{B}} > -27$) than those in our

³The magnitude limit used by SSG 95 of $M_{\text{B}} = -26.0$, who used $h_{70} = 57$, $m = 1$, $\beta = 0$ with $\beta = 0.5$, corresponds to $M_{\text{B}} = -26.47$ and -26.55 for our default cosmology and $\beta = 0.79$ at $z = 3$ and 5 respectively.

sample. Keeping this limitation in mind, we compare our result with the mean α_{ox} values in Tables 3 and A 1 in Vignali, Brandt, & Schneider (2003b) and Table 3 in Vignali et al. (2005), who used the same methods and assumptions as our work in deriving fluxes and α_{ox} values. Their Table A 1 includes recalculated α_{ox} values of $z > 4$ QSOs previously observed by Chandra (including those in Bechtold et al. 2003) using the same method. Their recalculations also took the time-dependent low-energy degradation of ACIS-S quantum efficiency into account. BALQSOs SDSS 1129-0142 and SDSS 1605-0122 (Vignali et al. 2003a) have been excluded from the following analysis, because BALQSOs are known to be X-ray weak due to a heavy absorption. Furthermore, we have derived X-ray fluxes of further three $z > 4$ QSOs from public archival Chandra ACIS-S data and calculated their α_{ox} values in the same way, as summarized in Table 3. The 1450 Å magnitudes of these three have been obtained from SSG 95 (PC 0910+5625) or the spectra from the SDSS DR3 database⁴ after corrections for Galactic extinction (the others). These three have been included in our statistical analysis.

The combined $z > 4$ sample is somewhat heterogeneous, as it consists of data obtained by a variety of programs, each with different interests and strategies. In our statistical analysis, we have divided the sample into five groups (Group A-E, with Group A being our $z \leq 3$ sample) as shown in Table 4. Figure 2 (b) shows the scatter diagram of the combined sample in the z – M_B plane with symbols showing the group membership. For each group, we have calculated the mean value $\langle \alpha_{\text{ox}} \rangle$ and the standard deviation of the mean. The combined sample includes five upper limit α_{ox} values (no X-ray detection) and we have used the Kaplan-Meier estimator to calculate the mean and standard deviation of the mean using the ASURV software (Feigelson & Nelson 1985), when necessary. Figure 2 (a) and (c) plots $\langle \alpha_{\text{ox}} \rangle$ of each group against z and M_B respectively.

Figure 2 (b) shows a rather incoherent scatter, reflecting the interests of individual original observing programs. As a result, z and M_B do not show strong monotonic z versus luminosity correlation, unlike flux-limited samples. This is for-

fortunate, because if such a correlation existed, it would be difficult to separate the redshift and luminosity dependences of α_{ox} .

Figs. 2 (a) and (c) seem to support the conclusion by (Vignali, Brandt, & Schneider 2003b) that the α_{ox} is anti-correlated with ultraviolet luminosity, while the correlation with z is weak, if any. We made a linear regression analysis of the dependent parameter α_{ox} against the two independent parameters, namely z and M_B . We also made separate one-independent parameter regressions for z or M_B versus the dependent parameter α_{ox} . The results of the analysis of the entire sample of 64 QSOs using the EM method available in ASURV (Isobe, Feigelson, & Nelson 1986) are shown below:

$$\alpha_{\text{ox}} = (1.662 \pm 0.028) + (0.042 \pm 0.027)(z - 4) + (0.071 \pm 0.019)(M_B + 27) \quad (1)$$

$$= (1.737 \pm 0.023) + (0.031 \pm 0.029)(z - 4) \quad (2)$$

$$= (1.648 \pm 0.049) + (0.068 \pm 0.019)(M_B + 27) \quad (3)$$

The coefficients for the regression analysis with the Buckley-James (B-J) and Schmitt's methods (if applicable) that are included in ASURV are consistent with those from the EM method shown above.

From either of Eqs. 1 & 3, we find a 3.5 dependence of α_{ox} to M_B . The slope coefficient can be translated into L_x / L_{opt} with $\alpha_{\text{ox}} = 0.56 \pm 0.12$ (from Eq. 3), that is consistent with the recent extensive analysis including lower redshift QSOs by Strateva et al. (2005).

⁴<http://www.sdss.org/>

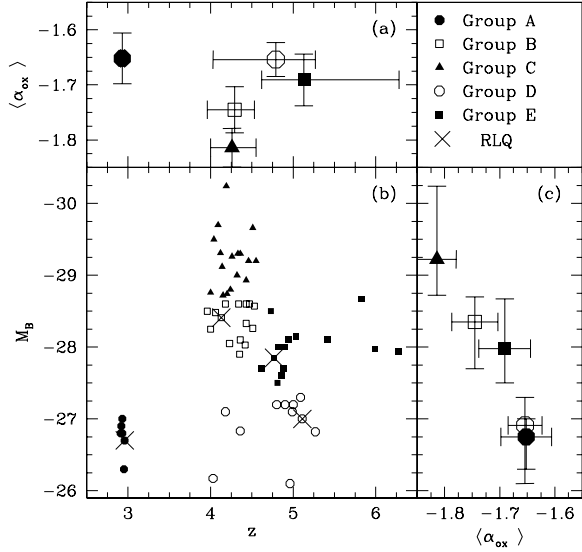


Fig. 2. | Grouping of QSOs from our sample and $z > 4$ samples from literature and $h_{\text{ox}i}$ of each group plotted against z and M_B . The QSOs are grouped according to the location in the $z\{M_B$ plane as plotted in panel (b). The groups are discriminated by different symbols as labeled. Radio-detected RLQs are indicated by a large cross. The $h_{\text{ox}i}$ value of each group is plotted against z and M_B in panels (a) and (c) respectively. Error bars of $h_{\text{ox}i}$ are the standard deviation of the mean and those of z and M_B are the range of these values in the group respectively. The data points for the groups are plotted with larger symbols than those for the individual QSOs.

4. Discussion

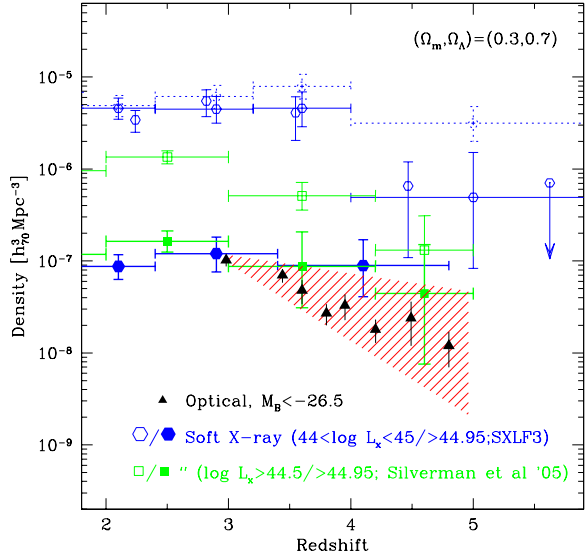


Fig. 3. | The number densities of soft X-ray selected QSOs from samples used by SXLF3 (blue hexagons) and Silverman et al. (2005) (green squares) are plotted with those of optically selected QSOs (SSG 95; Fan et al. 2001) (triangles), converted to our default cosmology. The X-ray luminosity cut ($\log L_x > 44.95$) was chosen to give the same number density as the optical curve at $z = 2.9$. The hatched area is a 90% confidence range of expected evolution of soft X-ray selected QSOs from the constraint on the systematic α_{ox} change with redshift as determined from the comparison between groups A & D. For reference, the density curves of QSOs from SXLF3 and Silverman et al. (2005) have been overplotted for the original paper's representative luminosity ranges as labeled and plotted in open symbols. The dotted data points from SXLF3 show the absolute maximum number densities where all the optically faint unidentified X-ray sources were at the center of the redshift bin.

Our primary goal of this study is to investigate the redshift dependence of α_{ox} between $z = 3$ and $z = 4$ to constrain the difference of number density behaviors of optically and X-ray selected QSOs at $M_B = -26.5$. In order to achieve this goal, we make more careful comparison of groups A (our sample) and D, which are well-separated in the redshift range (z_{hi} of 2.93 and 4.79 respec-

tively) and occupy approximately the same luminosity range (Fig. 2(b)). Since the difference in the mean M_B values for these two groups are small (≈ 0.16), the systematic difference of $\log_{10} L_x$ between these groups due to optical luminosity dependence is negligible (< 0.01 in $\log_{10} L_x$). The observed $\log_{10} L_x$ values of these groups are essentially the same. We have made Monte-Carb simulations to find the probability distribution of $\log_{10} L_x$, which is the difference between groups D and A to constrain the systematic change in $\log_{10} L_x$ with redshift at $z > 2.7$ at this luminosity range. In order to make a parent distribution of $\log_{10} L_x$ from which the simulations draw objects, we used the all QSOs in the current sample except for upper limits. Also $\log_{10} L_x$ of QSOs in each group have been shifted so that all groups have the same mean value. The standard deviation of these 58 $\log_{10} L_x$ values is consistent with those of groups A and D respectively. In each run, we randomly took 6 QSOs to represent group A and 11 to represent D respectively. The mean of each of the 6 and 11 random $\log_{10} L_x$ values has been calculated and the distribution of the difference of these means ($\log_{10} L_x$) for 2000 simulations have been investigated.

As a result, the range where 90% of the simulations fall in were $|\log_{10} L_x| < 0.13$. This limits the systematic difference in $\log(L_x=L_{\text{opt}})$ between $z \approx 3$ (group A) and $z > 4$ (group D) of 0.34 . For the slope of the luminosity function (LF) of $\alpha = 2$, this corresponds to a number density difference of $|\log_{10}(\rho_{\text{opt}} = \rho_x)| < 0.68$, where ρ_x and ρ_{opt} are the number densities of QSOs above optical luminosity and X-ray luminosities respectively. Figure 3 shows the evolution of comoving number density of soft X-ray selected QSOs (SXL3) as a function of redshift plotted with those of optical QSOs from SSG95 and Fan et al. (2001) at $z > 2.7$ (their original values are converted to our default cosmology and H_0). The luminosity limit for the soft X-ray QSOs is set at $\log L_x > 44.95$, where L_x is the observed frame $0.5-2$ keV in erg s^{-1} corresponding to approximately the 2.8 keV luminosity at the rest frame. Note that this is a rest-frame $0.5-2$ keV luminosity, under the assumption of $\alpha = 2.0$ power-law spectrum, which is representative of X-ray selected type 1 AGNs and SXL3 treats the luminosities as such. We also show the results from (Silverman et al. 2005)'s sample for the same observed $0.5-2$ keV

luminosity cut. This luminosity was selected such that the space density became equal to that of optical QSOs at $z = 2.7$ in thick lines and filled symbols. For reference, we show the number density curves from SXL3 and (Silverman et al. 2005) (open symbols with thin lines), in lower luminosity ranges (see labels), which are representative of the respective samples. These show declines in $z \geq 3$. The large error bars in the $\log L_x > 44.95$ data at $z > 2.7$ show that the QSOs in this regime is still underrepresented by current X-ray surveys. The limits of the number density curve of X-ray selected sample are shown in the shaded area in Fig. 3, corresponding to $|\log_{10} L_x| < 0.13$.

A limitation of the above investigation is the uncertainties in the effects of the sample selection and variability. The X-ray and optical luminosities have been measured in different epochs. Thus the variability of AGNs have a net effect of increasing the variance of the $\log_{10} L_x$ distribution. Our underlying assumption is that the variability does not cause a net systematic difference in its effect on the mean $\log_{10} L_x$ between sample A and sample D, separated in redshift, but not in luminosity. Both are optically selected samples and $\log_{10} L_x$ should be biased towards larger (more optically luminous) values than the "true" $\log_{10} L_x$ (i.e. $\log_{10} L_x$ of time-averaged mean optical and X-ray luminosities), because optical selection is more likely to pick up the AGN when it is more optically bright, while the X-ray follow up of the same object typically gives average X-ray luminosity of the source. As long as both are selected in the optical and followed up by X-ray, that the slope of the LF's are the same at both redshifts, and that there is no systematic difference in the variability amplitudes of AGNs with redshift, the effect of this "variability" bias should be the equal between sample A and sample D. Thus we do not expect that the variability bias plays a major role in our analysis on the redshift dependence of $\log_{10} L_x$.

From a combination of our sample at $z \approx 3$ and $z > 4$ QSOs observed by Chandra, we have confirmed the apparent dependence of $\log_{10} L_x$ on optical luminosity. This result, however, should be treated with caution, because our sample is optically selected and subject to the variability effect of preferentially picking up optically brighter phase as described above. An X-ray selected sample covering a much larger regime in $z-L$ space

rather showed L_x / L_{opt} (Hasinger 2005). This is, however subject to a similar effect working in the opposite sense. At this limited regime, on the other hand, there is a hint that our presently determined dependence might reflect the true behavior of the shift of α_x with QSO power. Expressing the LF as $d = d_0 \log L / L$ at the luminosities of interest, the soft X-ray LF has $\alpha_x = 2.2 \pm 0.3$ and (90% error) in $2.7 < z < 4.8$ (from the same sample as SXLF3). This can be compared with the optical LF of $\alpha_{\text{opt}} = 1.6 \pm 0.2$ (1 error) by Fan et al. (2001) or $\alpha_{\text{opt}} = 1.87$ by Schmidt, Schneider, & Gunn (1995). The trend that the optical LF has a flatter slope than the soft X-ray counterpart is consistent with the relation $\alpha_{\text{opt}} = \alpha_x$ within errors. This is also consistent with the comparison between X-ray and optically-selected AGN luminosity functions by Ueda et al. (2003) (see their Fig. 20), where a conversion of their hard X-ray LF to the optical band assuming $L_x / L_{\text{opt}}^{0.70}$ gave a good match to an observed optical QSO LF at high luminosities. However, our most recent comparison of the SXLF (Hasinger, Miyaji & Schmidt 2005) (high luminosity end) and optical QSO LF by Croom et al. (2004) at $z < 2.1$ is more consistent with L_x / L_{opt} , thus a more study is needed to investigate the relationship between direct comparison of L_x and L_{opt} and the conversion between the X-ray and optically selected QSO LFs.

5. Summary

We have made Chandra ACIS-S observations of six QSOs at $z \approx 3$, which marks the peak of luminous QSO number density. These observations fill a redshift gap in the X-ray coverage of luminous QSOs. We found an average photon index of $\langle \Gamma \rangle = 1.9 \pm 0.3$ from the stacked spectrum and we also found $\langle \alpha_x \rangle = 1.65 \pm 0.05$. The α_x value is essentially the same as those at $z > 4$ in the similar UV luminosity range and thus we have found no systematic shift of X-ray to UV luminosity ratios with redshift above $z = 3$. The density curves of $M_B < -26.5$ optically selected QSOs and $\log L_x > 44.92$ soft X-ray selected QSOs, giving the same densities at $z \approx 2.7$, are statistically consistent with each other within our limit of the systematic α_x shift at $z > 3$. We note that this regime is still underrepresented by X-ray surveys. Large-area moderately-deep X-ray surveys are needed to trace the rise of number density of

the most luminous QSOs at $z > 3$ in X-rays.

This work has been supported by Chandra General Observer Award GO3-4153X, NASA LTSA Grant NAG5-10875 (TM) and NSF grant AST03-07582 (DPS). We thank John Silverman for calculating the space density curves for our luminosity cuts and cosmological parameter choice.

REFERENCES

- Amaud, K., & Domnan, B. 2001, XSPEC Users Guide for version 11.1.x
- Barger, A. J., Cowie, L. L., Mushotzky, R. F., Yang, Y., Wang, W.-H., Steen, A. T., & Capak, P. 2005, *AJ*, 129, 578
- Bechtold, J., et al. 2003, *ApJ*, 588, 119
- Becker, R. H., White, R. L., & Helfand, D. J. 1995, *ApJ*, 450, 559
- Boyle, B. J., Shanks, T., & Peterson, B. A. 1988, *MNRAS*, 235, 935
- Cash, W. 1979, *ApJ*, 228, 939
- Condon, J. J., Cotton, W. D., Geisen, E. W., Yin, Q. F., Perley, R. A., Taylor, G. B., & Boderick, J. J. 1998, *AJ*, 115, 1693
- Cowie, L. L., Barger, A. J., Bautz, M. W., Brandt, W. N., & Gamire, G. P. 2003, *ApJ*, 584, L57
- Croom, S. M., Smith, R. J., Boyle, B. J., Shanks, T., Miller, L., Outram, P. J., & Loaring, N. S. 2004, *MNRAS*, 349, 1397
- Dickey, J. M., & Lockman, F. J. 1990, *ARA&A*, 28, 215
- Isobe, T., Feigelson, E. D., & Nelson, P. I. 1986, *ApJ*, 306, 490
- Fan, X., et al. 2001, *AJ*, 121, 54
- Feigelson, E. D., & Nelson, P. I. 1985, *ApJ*, 293, 192
- Fiore, F., et al. 2003, *A&A*, 409, 79
- Gamire, G. P., Bautz, M. W., Ford, P. G., Nousek, J. A., & Ricker, G. R. 2003, *Proc. SPIE*, 4851, 28

- Hasinger, G . 2005 in "Growing Black Holes" eds A .M erloni, S.N ayakshin and R .Sunyaev (Heidelberg:Springer), p418
- Hasinger, G ., M iya ji, T ., Schm idt, M . 2005, A & A , 441, 417
- M iya ji, T ., Hasinger, G . & Schm idt, M . 2000, A & A , 353, 25 (SXL F1)
- O sm er, P .S . 1982, ApJ, 253, 28
- Schneider, D .P ., Schm idt, M ., & Gunn, J.E . 1994, A J, 107, 1245
- Schneider, D .P ., et al. 2001, A J, 121, 1232
- Schmidt, M ., Schneider, D .P ., & Gunn, J.E . 1995, A J, 110, 68 (SSG 95)
- Shaver, P .A ., W all, J.V ., K ellem ann, K .I., Jackson, C .A ., & Hawkins, M .R .S . 1996, Nature, 384, 439
- Silverman, J.D ., et al. 2005, ApJ, 624, 630
- Strateva, I.V ., Brandt, W .N ., Schneider, D .P ., Vanden Berk, D .G ., & V ignali, C . 2005, A J, 130, 387
- Ueda, Y ., Akiyama, M ., Ohta, K ., & M iya ji, T . 2003, ApJ, 598, 886
- Vignali, C ., Brandt, W .N ., Fan, X ., Gunn, J.E ., Kaspi, S., Schneider, D .P ., & Strauss, M .A . 2001, A J, 122, 2143
- Vignali, C ., Brandt, W .N ., Schneider, D .P ., Garm ire, G .P ., & Kaspi, S. 2003a, A J, 125, 418
- Vignali, C ., Brandt, W .N ., & Schneider, D .P . 2003b, A J, 125, 433
- Vignali, C ., et al. 2003c, A J, 125, 2876
- Vignali, C ., Brandt, W .N ., Schneider, D .P ., & Kaspi, S. 2005, A J, 129, 2519
- W all, J.V ., Jackson, C .A ., Shaver, P .A ., Hook, I.M ., & K ellem ann, K .I. 2005, A & A , 434, 133
- W arren, S.J., Hewett, P .C ., & O sm er, P .S . 1994, ApJ, 421, 412
- W ilkes, B .J. 2000, in "Allen's Astrophysical Quantities, Fourth Edition" ed.A .N .Cox (New York:Springer), Chap. 24
- York, D .G ., et al. 2000, A J, 120, 1579
- Yuan, W ., Brinkmann, W ., Siebert, J., & Voges, W . 1998, A & A , 330, 108
- Yuan, W ., Siebert, J., & Brinkmann, W . 1998, A & A , 334, 498

This 2-column preprint was prepared with the AAS L^AT_EX macros v5.2.

Table 1
Log of Chandra Observations and Sample Properties

Name	Obsid/Date	Expo. (ks)	z	AB_{1450}^a	R_L
PC 0041+ 0215	4150/2003 Sep 01	9.2	2.93	19.5	< 1.5
PC 0947+ 5628	4151/2003 Jan 25	9.0	2.91	19.5	< 1.0
PC 1000+ 4751	4152/2002 Dec 18	13.9	2.95	20.0	< 1.2
PC 1015+ 4752	4153/2003 Jan 01	8.1	2.92	19.4	< 0.9
PC 1035+ 4747	4154/2003 Mar 16	10.0	2.96	19.6	2.3
PC 1447+ 4750	4155/2003 Jul 28	7.0	2.93	19.3	< 0.9

^aSome authors prefer to use the notation $AB_{1450(1+z)}$.

Table 2
X-ray Spectral Analysis Results and Derived Quantities

Name	z	$N_{\text{H};20}^{\text{G}}$ ^a		$S_{\text{x};14}^{\text{int}}$ ^b	$N_{\text{H};20}^{\text{z}}$ ^a	Scts	$\log L_{\text{x}}$ ^c	M_{B}	α_{x}
PC 0041+ 0215	2.93	2.8	2.4 (1.9;2.9)	1.4 (1.0;1.8)	0	36	45.0	26:8	1:56
PC 0947+ 5628	2.91	1.0	1.5 (0.7;2.3)	.31 (.17;.52)	0	10	44.4	26:8	1:78
PC 1000+ 4751	2.95	0.9	1.5 (1.2;1.9)	1.2 (1.0;1.5)	0	60	44.0	26:3	1:48
PC 1015+ 4752	2.92	1.0	2.4 (1.8;3.0)	.94 (.65;1.2)	0	24	44.9	26:9	1:64
PC 1035+ 4747	2.96	1.3	0.6 (0.3;1.4)	.17 (.08;.34)	0	9	44.3	26:7	1:80
PC 1447+ 4750	2.93	2.0	2.0 (1.4;2.6)	1.0 (.64;1.4)	0	21	44.9	27:0	1:65
h6 Q SO si	2.93	...	1.9 (1.7;2.1)	...	< 90		160	...	

Note. | The 90% confidence ranges and upper limits for one interesting parameter are shown for free parameters. Spectral parameters without a confidence range were fixed during the fit.

^aIn units of 10^{20} cm^{-2} .

^bX-ray flux before Galactic absorption in 0.5-2 keV (observer's frame), in units of $10^{-14} \text{ erg s}^{-1} \text{ cm}^{-2}$.

^cBase-10 logarithm of X-ray luminosity at the rest-frame 2-10 keV band in units of $h_{70}^2 \text{ erg s}^{-1}$.

Table 3
Additional Chandra Archival Data Analysis

Name	z	Obsid/Date (ks)	Expo.	$N_{H;20}^G$ ^a	$S_{x;14}^{int}$ ^{a b}	AB_{1450}	R_L	M_B	ox
PC 0910+ 5625	4.04	4821/2004 Mar 28	23.	2.9	1.7 (1.0;2.7)	20.7	< 1.5	-26.2	-1.67
SD SS J235718.36+ 004350.3	4.36	4827/2003 Nov 26	12.	3.3	5.0 (3.3;7.2)	20.2	< 1.2	-26.9	-1.56
SD SS J144428.67-012344.1	4.17	4826/2004 Jan 8	10.	4.0	1.8 (0.7;3.4)	19.8	< 1.2	-27.1	-1.79

^aSee notes to Table 2 for units.

^b90% confidence ranges are shown.

Table 4
Comparison of h_{ox}

group	$z_{m\ in}; z_{m\ ax}$	h_{zi}	$M_{B\ \mu\ in}; M_{B\ \mu\ ax}$	$hM_{B\ i}$	N_Q	$h_{ox\ i}^a$
A	2.9,3.0	2.93	27.0; 26.3	26.75	6	1.652 .046
B	3.5,4.6	4.29	28.7; 27.7	28.35	15	1.745 .042
C	3.5,4.6	4.26	30.3; 28.7	29.22	17	1.814 .035
D	4.0,5.3	4.79	27.5; 26.0	26.91	11	1.654 .031
E	4.6,6.4	5.13	28.8; 27.5	27.98	14	1.691 .047

^aThe errors are the standard deviation of the mean.